Eur. Phys. J. Plus (2016) **131**: 347
DOI 10.1140/epjp/i2016-16347-4

THE EUROPEAN PHYSICAL JOURNAL PLUS

Regular Article

The influence of a magnetic field on the heat transfer of a magnetic nanofluid in a sinusoidal channel

S. Valiallah Mousavi, M. Barzegar Gerdroodbary, Mohsen Sheikholeslami[a], and D.D. Ganji

Department of Mechanical Engineering, Babol Noshirvani University of Technology, Babol, Iran

Received: 29 March 2016 / Revised: 6 July 2016
Published online: 30 September 2016 –

Abstract. In this study, two dimensional numerical simulations are performed to investigate the influence of the magnetic field on the nanofluid flow inside a sinusoidal channel. This work reveals the influence of variable magnetic field in the heat transfer of heat exchanger while the mixture is in a single phase. In this heat exchanger, the inner tube is sinusoidal and the outer tube is considered smooth. The magnetic field is applied orthogonal to the axis of the sinusoidal tube. In our study, the ferrofluid (water with 4 vol% nanoparticles (Fe_3O_4)) flows in a channel with sinusoidal bottom. The finite volume method with the SIMPLEC algorithm is used for handling the pressure-velocity coupling. The numerical results present validated data with experimentally measured data and show good agreement with measurement. The influence of different parameters, like the intensity of magnetic field and Reynolds number, on the heat transfer is investigated. According to the obtained results, the sinusoidal formation of the internal tube significantly increases the Nusselt number inside the channel. Our findings show that the magnetic field increases the probability of eddy formation inside the cavities and consequently enhances the heat transfer (more than 200%) in the vicinity of the magnetic field at low Reynolds number ($Re = 50$). In addition, the variation of the skin friction shows that the magnetic field increases the skin friction (more than 600%) inside the sinusoidal channel.

Nomenclature

(a.b)	center of magnetic wire (m)
A	dimensionless wavy amplitude ($A = \delta/r_i$)
C_f	skin-friction coefficient
C_p	specific heat (J/kg K)
D_h	hydraulic diameter (m)
d_p	magnetic particle diameter (m)
H_r	characteristic magnetic field strength (A/m)
H_x	magnetic field intensity component in the x-direction (A/m)
H_y	magnetic field intensity component in the y-direction (A/m)
I	electric intensity (A)
k	thermal conductivity (W/m °C)
k_B	Boltzmann constant ($1.3806503 \times 10^{-23}$ J/K)
L_w	wavelength of the wavy wall (m)
M	magnetization (A/m)
Mn	magnetic number
m_p	particle magnetic moment (A m^2)
Nu	Nusselt number
q_w	wall heat flux (W/m^2)
Re	Reynolds number
T	temperature °C
x^*	dimensionless axis in the Cartesian coordinates ($x^* = x/r_i$)
y^*	dimensionless axis in the Cartesian coordinates ($y^* = y/r_i$)
z^*	dimensionless axis in the Cartesian coordinates ($z^* = z/r_i$)

Greek symbols

δ	wavy amplitude (m)
$\emptyset$	volume fraction of particles (%)
μ	dynamic viscosity (N s/m^2)
μ_0	magnetic permeability in vacuum ($4\pi \times 10^{-7}$ TA/m)
μ_B	Bohr magneton (9.27×10^{-24} A m^2)
ρ	density (kg/m^3)
θ^*	dimensionless temperature (T/T_0)

Subscripts

avg	average
f	pertaining to base fluid
p	pertaining to magnetic particles
m	pertaining to mixture
0	pertaining to inlet conditions

[a] e-mail: m.sheikholeslami@stu.nit.ac.ir

1 Introduction

A magnetic nanofluid (ferrofluid) is a magnetic colloidal suspension consisting of a base liquid and magnetic nanoparticles with a size range of 5–15 nm in diameter coated with a surfactant layer. Heat exchangers are used in various applications in engineering systems, such as food industry, power generation, heat recovery systems, process plants, etc. Sinusoidal double pipes are well-known types of curved tubes; they are used in air-conditioning and refrigeration systems, heat recovery processes and chemical reactors due to their high heat transfer coefficient. Recently, the presence of the nanofluid in the heat exchangers highly enhances the performance of this instrument [1]. Furthermore, the importance of this type of heat exchanger is significantly increased as the magnetic field is presented [2].

For more than a decade, magnetic nanoparticles concepts have been studied as a means to modify or enhance the heat transfer on various applications and devices [1–7]. Recently, scientists and researchers focus on the influence of the magnetic field on the heat transfer of magnetic nanoparticles. Jue [1] used the semi-implicit finite element method in order to simulate a magnetic gradient and thermal buoyancy induced cavity ferrofluid flow. His results showed that the flow strength increases with strengthening the magnetic field. Numerical analysis of the heat transfer enhancement and fluid flow characteristics of a rotating cylinder under the influence of magnetic dipole in the backward facing step geometry was conducted by Selimefendigil and Oztop [2]. They found that the effect of the cylinder rotation on the local Nusselt number distribution is more pronounced at low Reynolds number. Nanjundappa *et al.* [3] studied the effect of magnetic-field–dependent (MFD) viscosity on the onset of ferroconvection in a ferrofluid-saturated horizontal porous layer. They showed that an increase in the porous parameter, MFD viscosity parameter and a decrease in the magnetic number is to delay the onset of ferroconvection, while the nonlinearity of fluid magnetization has no influence on the stability of the system. The vortex dynamics behind various magnetic obstacles and the characteristics of heat transfer were investigated by Zhang and Huang [4]. They found that the pressure drop penalty is not increasingly reliant on interaction parameter. Azizian *et al.* [5] studied the effect of an external magnetic field on the convective heat transfer and pressure drop of magnetite nanofluids under laminar flow regime conditions. They worked on the simulation of magnetic field and magnetic force distribution and showed that the mechanisms of heat transfer enhancement are postulated to be an accumulation of particles near the magnets (leading to higher thermal conductivity locally). Sheikholeslami *et al.* [6] studied the MFD viscosity influence on the nanofluid free convection. They proved that the MFD viscosity effect is more pronounced for low Hartmann number. Sheikholeslami *et al.* [7] examined the nanofluid radiation heat transfer in the presence of a magnetic field. Aursand *et al.* [8] proposed a multi-phase flow model for a thermomagnetically pumped ferrofluid. Their results indicated a very large sensitivity to uncertainties in heat transfer coefficient predictions. Rahman *et al.* [9] studied the augmentation of natural convection heat transfer in the triangular shape solar collector by utilizing water-based nanofluids with a corrugated bottom wall. They found that both Grashof number and solid volume fraction have a significant influence on streamlines and isotherms in the enclosure. The effects of using different geometrical parameters with the combination of a nanofluid on heat transfer and fluid flow characteristics in a helically coiled tube heat exchanger (HCTHE) were numerically investigated by Mohammed and Narrein [10]. They showed that counter-flow configuration produced better results as compared to parallel-flow configuration. Sheikholeslami *et al.* [11] presented the influence of a variable magnetic field on the forced convection heat transfer. Hosseini *et al.* [12] investigated rheological properties and magnetoviscous effects of magnetic Ni nanoparticles. Their results clearly confirmed that these ferrofluids are non-Newtonian fluids for all nanoparticles concentrations. Forced convection and pressure drop of a Fe_3O_4 nanofluid under an external magnetic field were studied experimentally by Goharkhah *et al.* [13]. They found that an increase of the pressure drop is an inevitable effect of applying a magnetic field to the ferrofluid. In the recent decade, several researchers studied about magnetic nanofluid [14–26].

The main purpose of the present work is to study ferrofluid flow and heat transfer in a sinusoidal channel in the presence of an external magnetic field. FVM is applied to solve this problem. Initially, the sinusoidal channel is simulated to investigate the influence of the geometry on the thermal performance of the channel. In addition, the feature of the stream inside the cavity of the channel is studied comprehensively. Then, the magnetic field is presented and the influence of the magnetic field with various nanofluids inlet conditions are investigated and revealed the effects of the magnetic field on the temperature and convection performance of surfaces. Finally, the temperature distribution in the sinusoidal channel in different external magnetic field is compared.

2 Theoretical formulation

2.1 Geometry and grid

Figure 1(a) illustrates the schematic of the sinusoidal channel in the presence of the wire orthogonal to the axis of the channel. The magnetic field is generated by an electric current going through a thin and straight wire oriented orthogonal to the longitudinal axis (x) at the position (a, b) and the current in the wire flows in the direction of the positive z-axis. The structure of the magnetic field in the vicinity of the wire is depicted in the fig. 1(b).

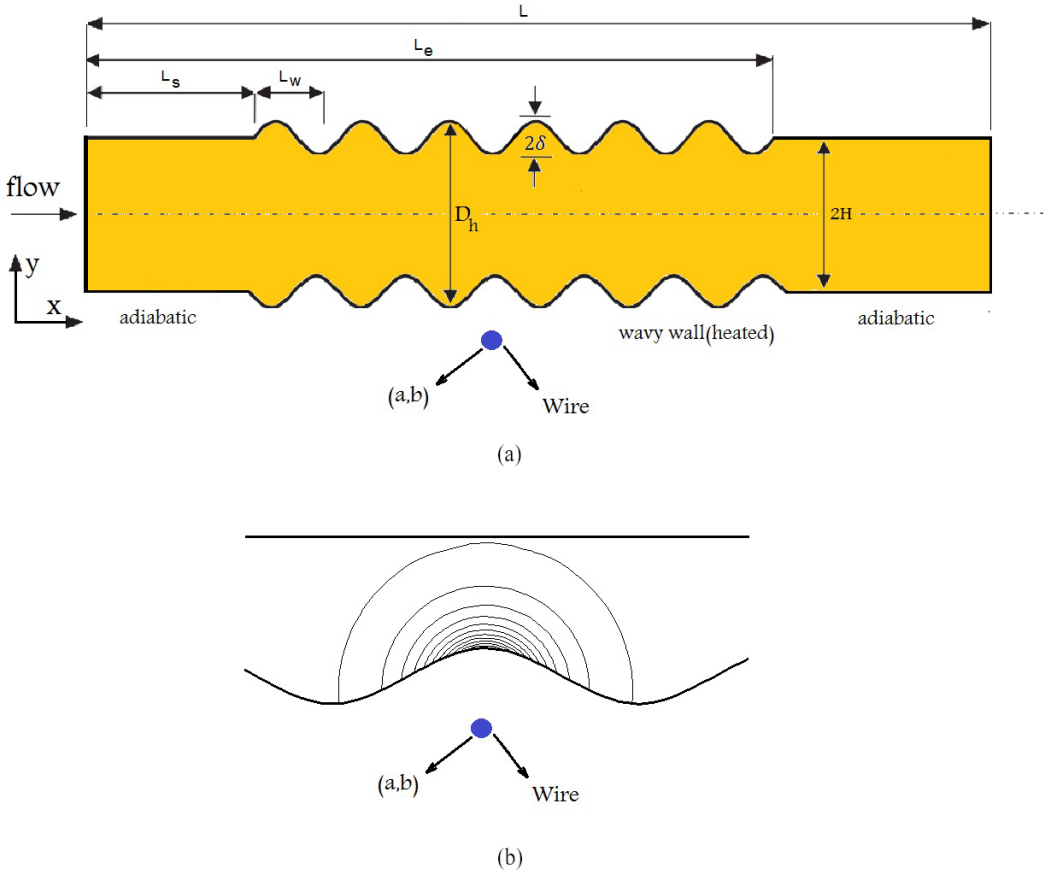

Fig. 1. (a) Three-dimensional sinusoidal channel with magnetic field carrying wire. (b) The effect of magnetic field intensity on the ferrofluid of inside channel.

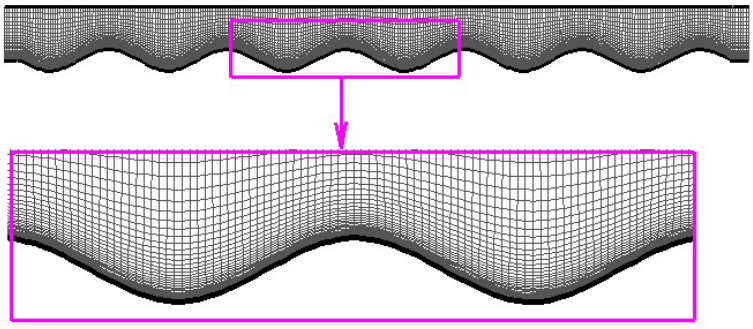

Fig. 2. Grid.

As is shown in fig. 1(a), the length of the channel is L with inner diameter 2H and the amplitude of electric current is (δ) with wavelength of (L_w). The total length of the wavy wall is six wavelengths, *i.e.* there are six waves along the wavy wall. In addition, the profile of the lower wavy wall can be represented by

$$S(z) = -\frac{d_i}{2} - \delta \sin\left[\frac{2\pi(z - L_s)}{L_w}\right], \quad L_s \leq z \leq L_e. \tag{1}$$

Figure 2 illustrates a sample grid inside the channel. In this study, a fully structured grid is generated to reduce the errors, especially in the vicinity of the sinusoidal wall of the constructed model. As is shown in the figure, the grid refinement was obtained manually in the region immediately close to the bottom wall. An example of the grid in the vicinity of a sinusoidal wall is also depicted in fig. 2.

One of the primary factors for the evaluation of the numerical studies is the proper grid resolution. Therefore, an extensive grid refinement study (mesh number from 11850 to 30000) was implemented to determine grid independence

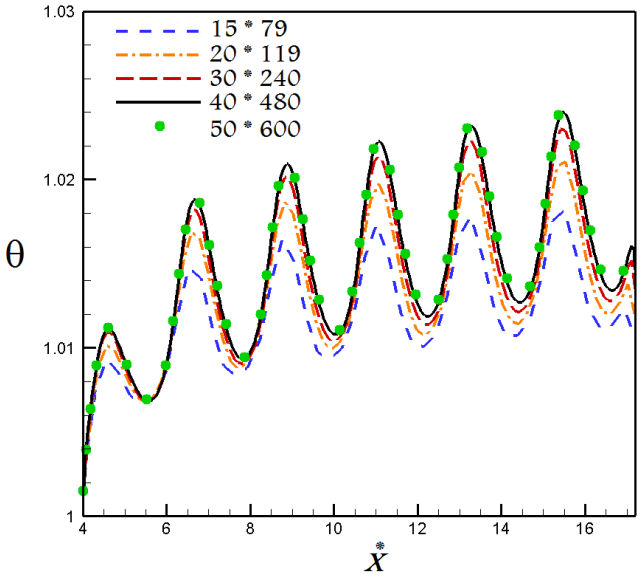

Fig. 3. Grid independence.

in temperature distribution in the axial direction of the channel (x) (fig. 3). It is found that fine grid (19200) with 40 cells in the y-direction and 480 cells in the x-direction has enough precision and acceptable convergent time for the present investigation.

2.2 Governing equations and numerical methods

In this study, Navier-Stokes equations and energy equations are coupled to obtain flow feature and heat transfer inside the sinusoidal channel. To investigate the influence of the magnetic field, the components of the magnetic field should be taken into account in the momentum equations. Moreover, it is assumed that the physical properties of the fluid are constant. The effects of magnetic fields on the viscosity and the thermal conductivity of the ferrofluid have been assumed to be negligible. It should be mentioned that the non-uniform transverse magnetic field has a negligible effect in MHD, and the Lorentz force is also considered negligible compared to the magnetic force due to the electrical conductivity. Moreover, dissipation and pressure work is ignored in the present study. Considering these assumptions the two-dimensional conservation equations for the steady-state condition are as follows.

Continuity equation:

$$\frac{\partial u}{\partial x}+\frac{\partial v}{\partial y}=0. \tag{2}$$

Momentum equation:

$$\rho_m\left(u\frac{\partial u}{\partial x}+v\frac{\partial u}{\partial y}\right)=-\frac{\partial p}{\partial x}+\mu_m\left(\frac{\partial^2 u}{\partial x^2}+\frac{\partial^2 u}{\partial y^2}\right)+F_K(x) \tag{3}$$

$$\rho_m\left(u\frac{\partial v}{\partial x}+v\frac{\partial v}{\partial y}\right)=-\frac{\partial p}{\partial y}+\mu_m\left(\frac{\partial^2 v}{\partial x^2}+\frac{\partial^2 v}{\partial y^2}\right)+F_K(y). \tag{4}$$

Energy equation:

$$(\rho_m C_p)_m\left(u\frac{\partial T}{\partial x}+v\frac{\partial T}{\partial y}\right)=k_m\left(\frac{\partial^2 T}{\partial x^2}+\frac{\partial^2 T}{\partial y^2}\right). \tag{5}$$

The term $F_K(x)$ and $F_K(y)$ are related to FHD due to the existence of the magnetic gradient and are called the Kelvin force. $\mu_0 M\frac{\partial H}{\partial x}$ and $\mu_0 M\frac{\partial H}{\partial y}$ are the components of the Kelvin force in the x and y directions, respectively. They resulted from the electric current flowing through the wire. Therefore, it is needed to define the magnetic field of electric current. The components of the magnetic field H_x, H_y in the x and y directions are calculated as follows [27]:

$$H_x(x,y)=\frac{I}{2\pi}\frac{(x-a)}{(x-a)^2+(y-b)^2} \tag{6}$$

$$H_y(x,y)=\frac{I}{2\pi}\frac{(y-b)}{(x-a)^2+(y-b)^2}. \tag{7}$$

The magnitude of the magnetic field intensity is given by

$$H(x,y,z) = \frac{I}{2\pi} \frac{1}{\sqrt{(x-a)^2 + (y-b)^2}}\,. \tag{8}$$

We need to mention that the term $\mu_0 M \frac{\partial H}{\partial z}$ should be added to the momentum equation in the z-direction when axial non-uniform magnetic gradient is in the domain. M is the magnetization and is defined as [28]

$$M = \frac{6m_p}{\pi d_p^3} \left[\coth h(\xi) - \frac{1}{\xi}\right]. \tag{9}$$

The unit cell of the crystal structure of magnetite has a volume of about $730\,\mathrm{A}^3$ and contains 8 molecules of Fe_3O_4; each of them has a magnetic moment of $4\mu_B$ [29]. Therefore the particle magnetic moment for the magnetite particles is obtained as

$$m_p = \frac{4\mu_B \pi d_p^3}{6 \times 91.25 \times 10^{-30}}\,. \tag{10}$$

Also ξ is the Langevin parameter and is defined as [28]

$$\xi = \frac{\mu_0 m_p H}{k_B T}\,. \tag{11}$$

It is also noted that the dimensionless magnet number (Mn) is used to measure and the effect of the magnetic field intensity. The magnetic number (Mn) is dependent on the magnetic field intensity. This means that Mn increases with an increase in the magnetic field intensity,

$$Mn = \frac{\mu_0 \chi H_r^2 h^2}{\rho_m \alpha_m^2}\,, \tag{12}$$

where χ is the magnetic susceptibility of the ferrofluid. As mentioned earlier, the magnetic susceptibility of a ferrofluid containing 4 vol% with a mean diameter of 10 nm is in the order of $\chi = 0.348586$ [30]. H_r is the characteristic of magnetic field strength and is calculated by $H_r = H(a,0) = \frac{I}{2\pi b}$. The mixture physical properties in the above equations are calculated as below.

Mixture density [31]:

$$\rho_m = \varphi \cdot \rho_p + (1-\varphi) \cdot \rho_f. \tag{13}$$

Mixture dynamic viscosity:

$$\mu_m = \frac{1}{(1-\varphi)^{2.5}} \mu_f. \tag{14}$$

Mixture thermal conductivity for spherical nanoparticles [32]:

$$k_m = \left[\frac{k_p + 2k_f - 2\varphi(k_f - k_p)}{k_p + 2k_f + \varphi(k_f - k_p)}\right] k_f. \tag{15}$$

Mixture specific heat:

$$cp_m = \varphi \cdot cp_p + (1-\varphi) \cdot cp_f. \tag{16}$$

The Reynolds number and Nusselt number, as two main non-dimensional numbers, are calculated by the following equation:

$$Re_m = \frac{\rho_m v_m d_i}{\mu_m} \tag{17}$$

$$Nu_{hot} = \frac{q'' D_{h_i}}{k_m (T_w - T_b)}\,, \tag{18}$$

where D_{h_i} is expressed by the following equation:

$$D_{h_i} = d_i + 2\delta. \tag{19}$$

In the present study, the second-order upwind numerical scheme decoupling with the SIMPLEC algorithm is used, and all the governing equations are solved through a finite volume CFD code [33–36].

Table 1. Properties of the studied fluid and particles.

	$\rho\left(\frac{\text{kg}}{\text{m}^3}\right)$	$C_p\left(\frac{\text{J}}{\text{kg}\cdot\text{K}}\right)$	$k\left(\frac{\text{W}}{\text{m}\cdot{}^\circ\text{C}}\right)$	$\mu\left(\frac{\text{N s}}{\text{m}^2}\right)$
Copper	8978	381	387.6	–
Fe_3O_4 (p)	5200	670	6	–
Water (f)	1024	4001.1	0.596	0.00108

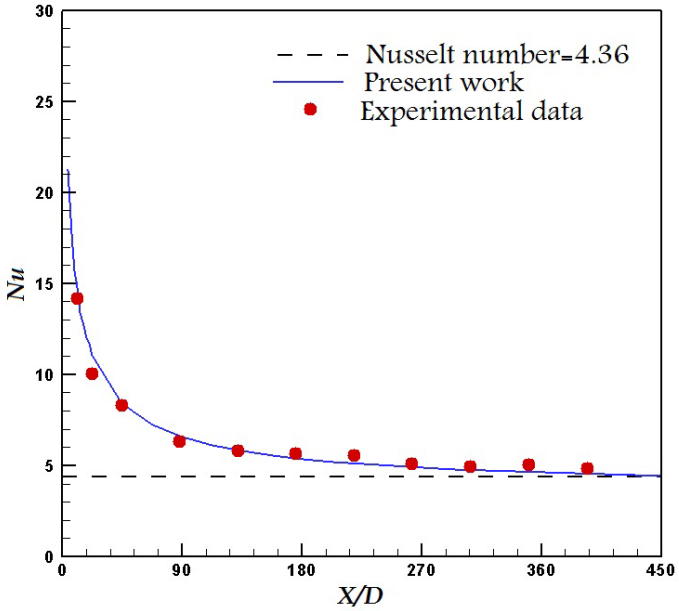

Fig. 4. Comparison of the results obtained for water in a horizontal pipe.

2.3 Flow and boundary conditions

The inflow conditions of the ferrofluid are equivalent to $Re_m = 50$, 100, 150 and 200 with constant temperature ($T_{in} = T_0$). Various magnetic numbers ($Mn = 0$, $8.28e+6$, $18.64e+6$ and $33.16e+6$) are examined to reveal different aspects of the magnetic strength on the heat transfer inside the sinusoidal channel. Also, for studying heat transfer, results of the Nusselt number have been presented for a water-based ferrofluid containing of 4 vol% Fe_3O_4 spherical shape particles with 10 nm mean diameter. Properties of the studied fluid and particles are presented in table 1.

3 Results

3.1 Validation

Validation of the results is realized with a numerical simulation of Kim *et al.* [37] experimental test runs. In order to show the validation of the present model, the flow fluid and heat transfer of water in a pipe at $Re = 1620$ is studied. In this model, the wall of the pipe is under a constant heat flux. Figure 4 compares the obtained results from numerical solution of this problem with the experimental data of Kim *et al.* [37] at constant Nusselt number ($Nu = 4.36$).

Further investigation is conducted on a vertical pipe under the magnetic field effect where the Reynolds number of the nanofluid is $Re = 40$. As shown in fig. 5, the velocity results show good agreement with those of Aminfar *et al.* [38].

3.2 Results of numerical simulations

In this section, the effects of different parameters, like Reynolds number and magnetic number, on the heat transfer of the ferrofluid are comprehensively studied. Figure 6 compares the influence of the magnetic field on streamlines

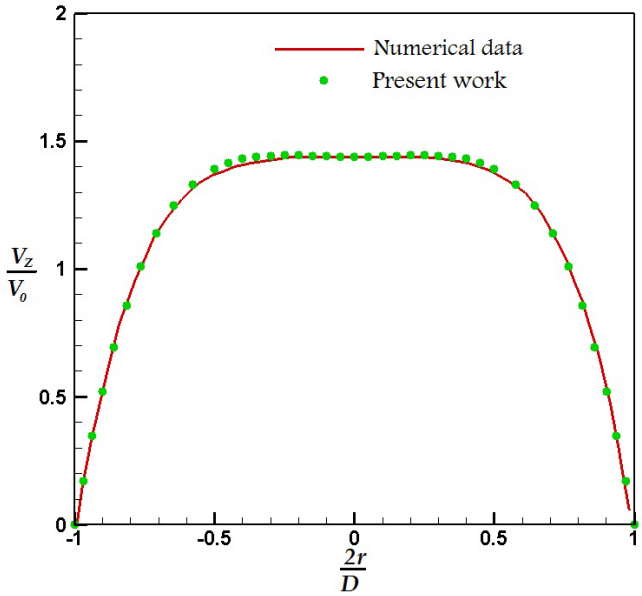

Fig. 5. Comparison of the results obtained for the ferrofluid.

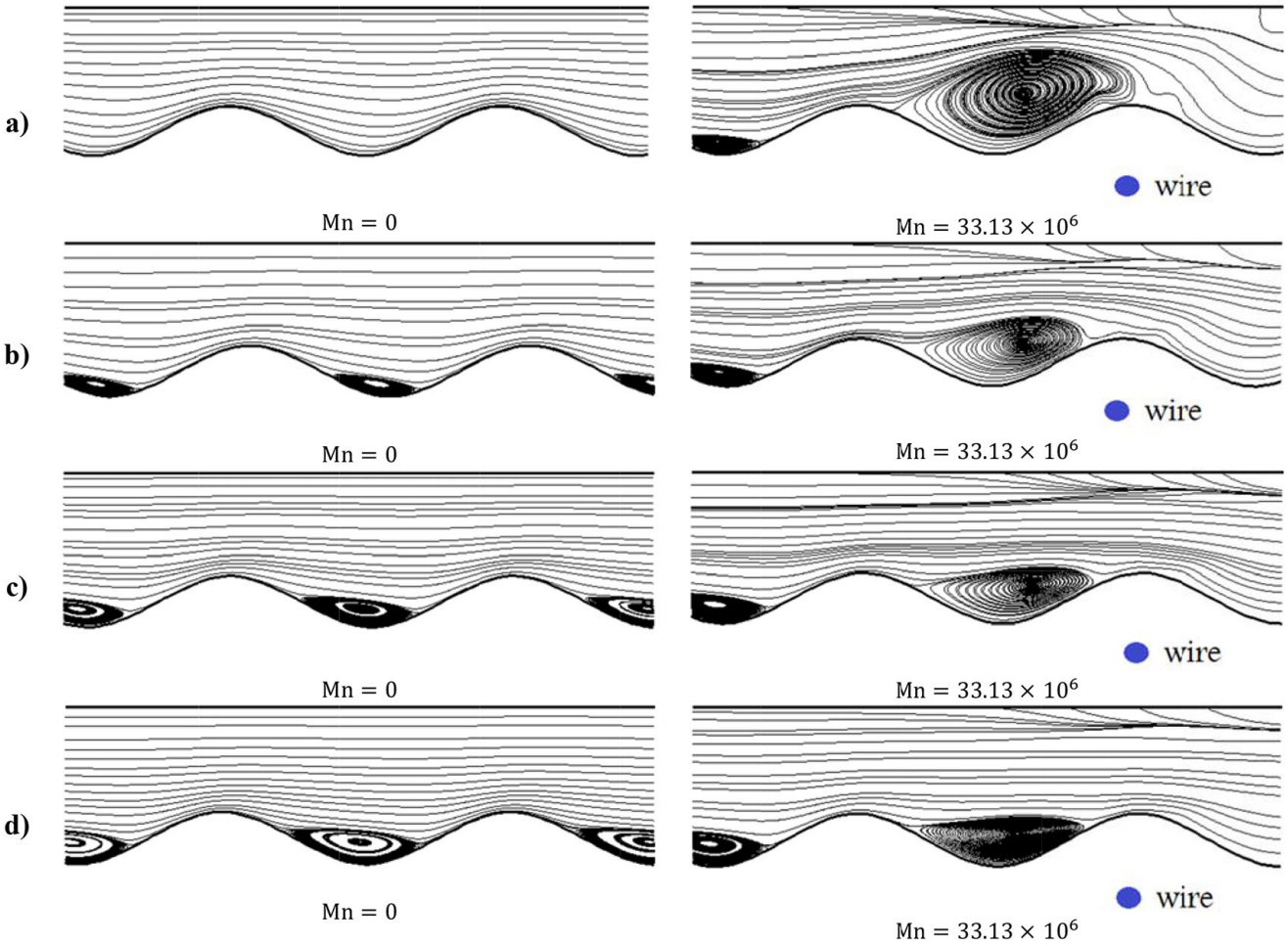

Fig. 6. Comparison of streamlines inside the sinusoidal channel for (a) $Re = 50$, (b) $Re = 100$, (c) $Re = 150$, (d) $Re = 200$ with/without constant magnetic field $Mn = 33.13 \times 10^6$.

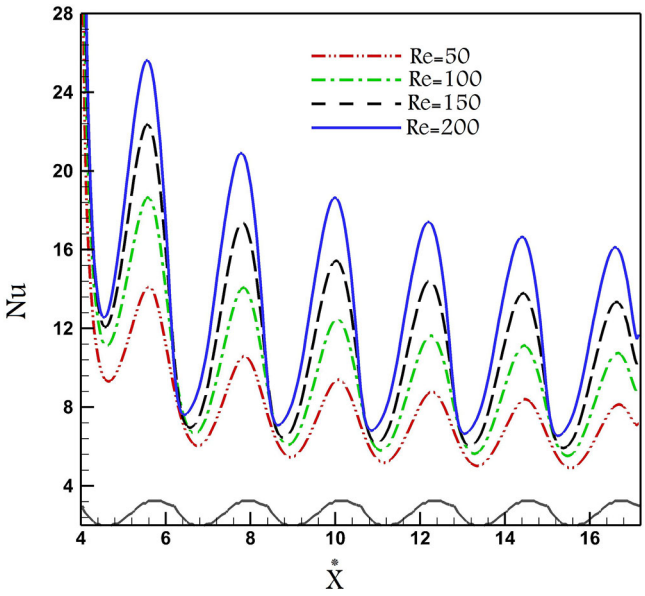

Fig. 7. Comparison of the Nusselt number inside the sinusoidal channel at $Re = 50$, 100, 150 and 200 without magnetic field.

patterns of the nanofluid inside cavities with different Reynolds numbers. The presence of a cavity led to the generation of eddies at high Reynolds number. Since an adverse pressure gradient is formed as a result of geometric non-uniformity (*i.e.* the sinusoidal shape), the separation is clearly discerned in the domain. The production of eddies as a result of separation in cavities results in an increase in the heat transfer rate.

As the magnetic field is presented in the orthogonal direction of the channel, a large eddy is clearly noticed at low Reynolds number. In fact, the magnetic field intensifies the adverse pressure gradient, which increases the probability of the eddy formation. Since the momentum of the main stream is small at low Reynolds number ($Re = 500$), a large eddy is formed in the cavity. By increasing the inflow velocity, the size of the eddy is reduced due to the high momentum of the inflow.

In order to realize the influence of the sinusoidal shape of the channel on the heat transfer, the variation of the Nusselt number along the axis of the channel without magnetic field is illustrated in fig. 7 for various Reynolds numbers. The figure obviously shows that the effects of the Reynolds number are more significant at maximum Nusselt number. In addition, the Nusselt number highly increases when the Reynolds number is higher. The Nusselt number has a periodically decreasing behavior from the beginning of the sinusoidal part of the pipe. Also, increasing the Reynolds number moves the separation point toward the crest of the sinus wave in the diverging part of the pipe.

Figure 8 plots the Nusselt number along the axis of the channel for various Reynolds numbers with four different magnetic numbers ($Mn = 0$, $8.28e+6$, $18.64e+6$ and $33.16e+6$). It can be observed that the magnetic field enhances the velocity gradient near the wall and hence results in an increase in the Nusselt number. Furthermore, it is clearly perceived that the intensity of the heat transfer significantly increases when the inflow velocity is low.

Skin friction plays a significant role in the heat transfer of flow in different geometries exclusively inside the channel. Moreover, the main feature of the internal flow highly relies on the friction of the surface. Hence, the variation of the skin friction along the axis of the channel is compared in fig. 9 for various Reynolds numbers. It is clear that the value of skin friction unexpectedly increases when the flow coincides with the maximum height of the channel. This increase intensifies with high inflow velocity. In addition, the maximum skin friction becomes constant as the flow passes a few sinusoidal waves in the channel.

Figure 10 depicts the variation of the skin friction along the channel in the presence of the non-uniform magnetic field with various strengths. The figure shows that the skin friction unexpectedly increases in the presence of the magnetic field. In fact, the quantitative analysis of the skin friction shows that the value of the skin friction intensifies more than 6 to 7 times in the vicinity of the magnetic field on the maximum height of the channel. This increase in the skin friction augments the adverse pressure gradient and eddies are formed inside the cavity.

Since the electrical wire produces a non-uniform magnetic field in the x and y directions, the influence of the magnetic field is not limited. The cavities close to the main cavity are highly affected. As the magnetic field intensity increases, the velocity decreases. This increase results in a secondary flow, which appears as two eddies.

The temperature contour of the nanofluid along the sinusoidal channel with/without magnetic source is depicted in fig. 11. As mentioned before, the non-dimensional temperature ($T^* = \frac{T}{T_{inlet}}$) is highly influenced by the magnetic

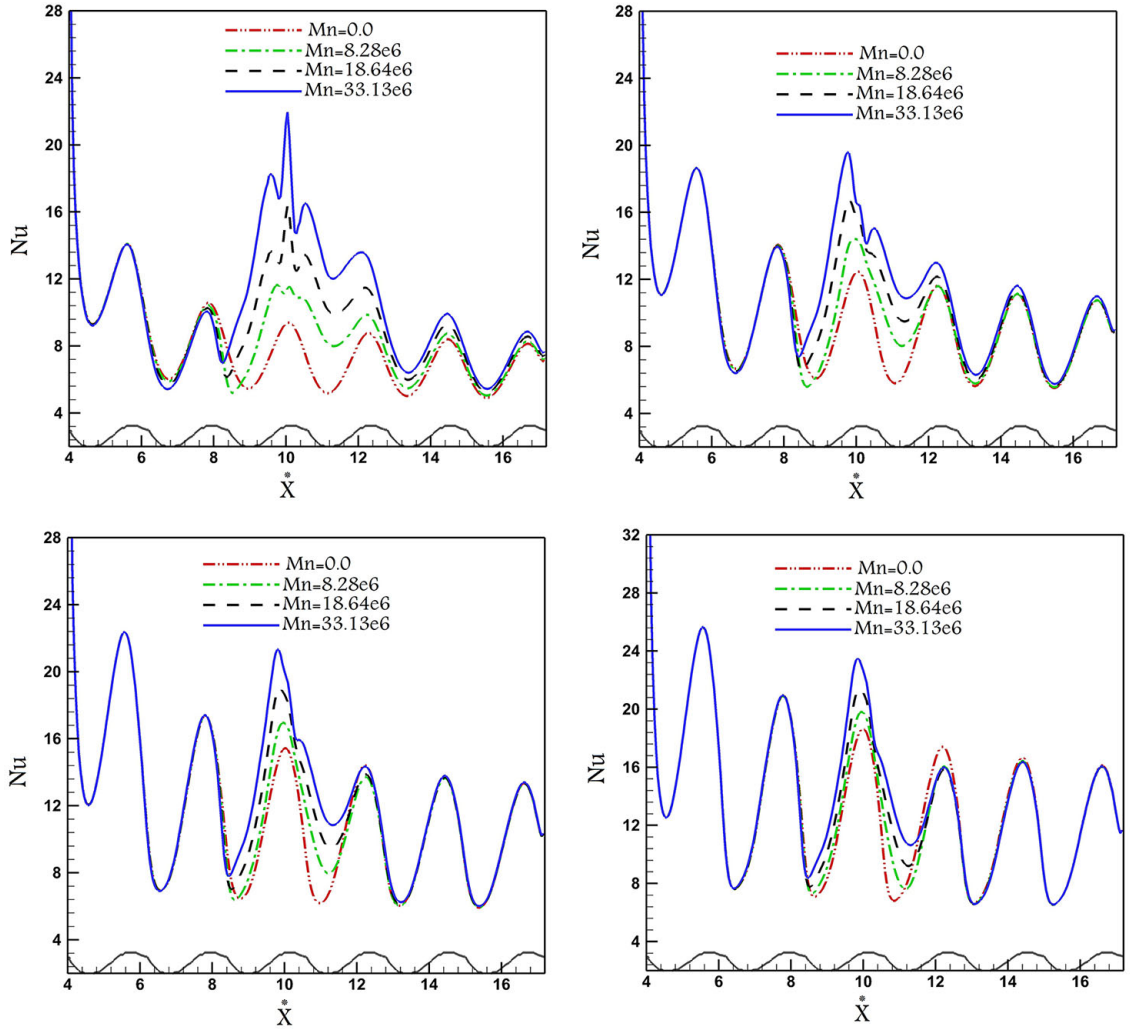

Fig. 8. Comparison of the Nusselt number inside the sinusoidal channel at (a) $Re = 50$, (b) $Re = 100$, (c) $Re = 150$, (d) $Re = 200$, with varying magnetic field ($Mn = 0$, $8.28e+6$, $18.64e+6$ and $33.16e+6$).

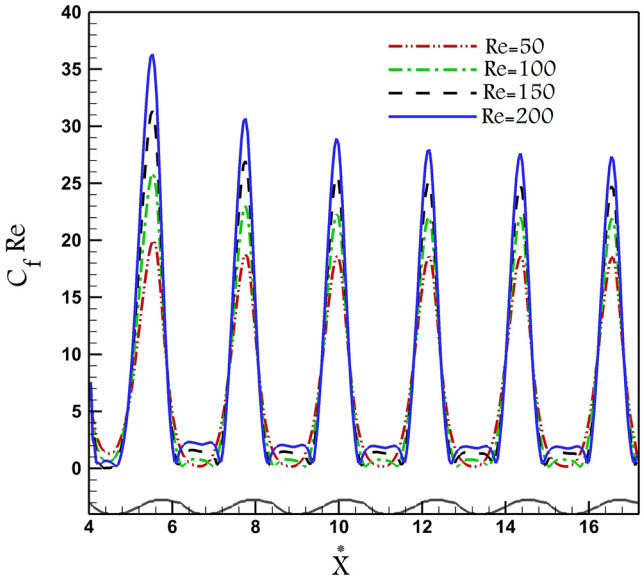

Fig. 9. Comparison of the skin friction inside the sinusoidal channel at $Re = 50$, 100, 150 and 200 without magnetic field.

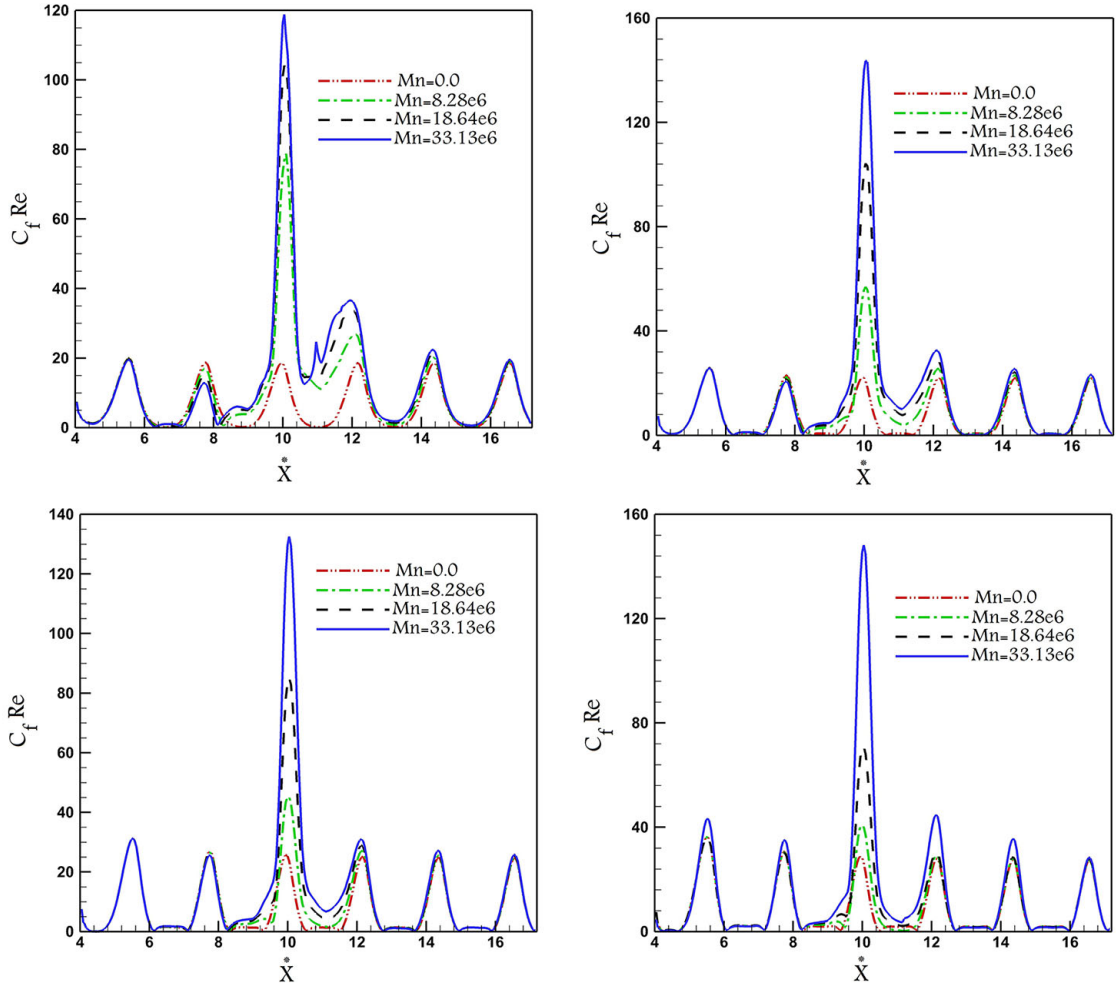

Fig. 10. Comparison of skin friction inside the sinusoidal channel at (a) $Re = 50$, (b) $Re = 100$, (c) $Re = 150$, (d) $Re = 200$, with varying magnetic field ($Mn = 0$, $8.28e + 6$, $18.64e + 6$ and $33.16e + 6$).

field at low Reynolds number ($Re = 50$). Since the large eddy is formed in the cavity close to a magnetic field, the temperature significantly decreases in this region in comparison with the case with no magnetic field. As the velocity of the inlet flow increases, the influence of the magnetic field on the temperature reduces. In fact, forced convection plays the main role in the temperature distribution of the channel.

4 Conclusion

In this article, a numerical investigation was performed on the nanofluid magnetic flow in a sinusoidal channel under variable magnetic field. The obtained results show that the sinusoidal plate significantly enhances the heat transfer in the channel. In fact, this effect is due to the entrainment of the ferrofluid in cavities of the base channel. This study reveals various aspects of the magnetic field on the flow feature and temperature distribution inside the channel. Our findings show that the Nusselt number increases more than 200% in the vicinity of magnetic field (with $Mn = 33.13 \times 10^6$) at low Reynolds number ($Re = 50$). In addition, the flow features are highly influenced by increasing magnetic field intensity due to the extension of the eddy in the cavity. The variation of the skin friction shows that this factor increases by more than 6 times as the magnetic field ($Mn = 33.13 \times 10^6$) is presented. According to our results, the presence of the magnetic field significantly increases the heat transfer and consequently enhances the cooling performance in the sinusoidal channel.

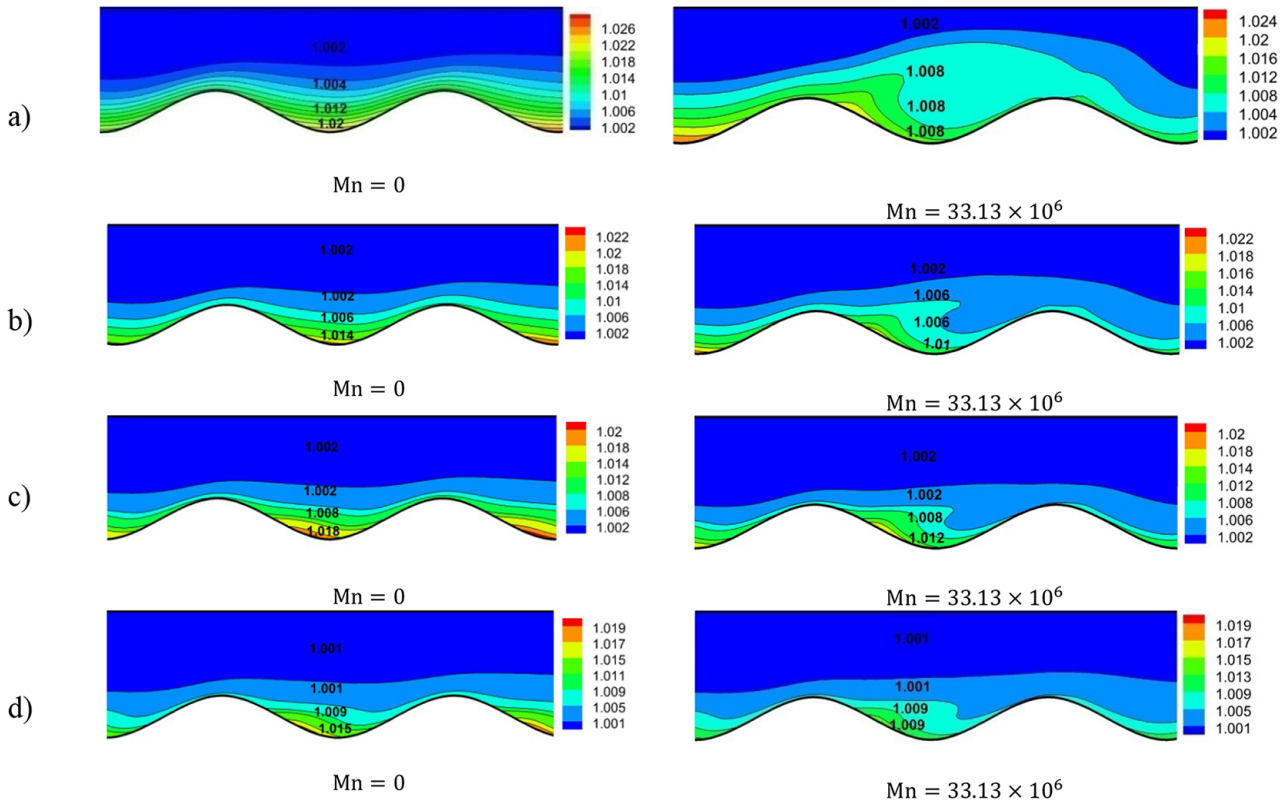

Fig. 11. Comparison of non-dimensional temperature inside the sinusoidal channel at (a) $Re = 50$, (b) $Re = 100$, (c) $Re = 150$, (d) $Re = 200$, with/without constant magnetic field $Mn = 33.13 \times 10^6$.

References

1. T.Ch. Jue, Int. Commun. Heat Mass Transf. **33**, 846 (2006).
2. F. Selimefendigil, H.F. Oztop, Int. J. Heat Mass Transf. **71**, 142 (2014).
3. C.E. Nanjundappa, I.S. Shivakumara, M.M. Ravisha, Int. Commun. Heat Mass Transf. **37**, 1246 (2010).
4. X. Zhang, H. Huang, Int. Commun. Heat Mass Transf. **51**, 31 (2014).
5. R. Azizian, E. Doroodchi, T. McKrell, J. Buongiorno, L.W. Hu, B. Moghtaderi, Int. J. Heat Mass Transf. **68**, 94 (2014).
6. M. Sheikholeslami, M.M. Rashidi, T. Hayat, D.D. Ganji, J. Mol. Liq. **218**, 393 (2016).
7. M. Sheikholeslami, M. Gorji-Bandpy, Powder Technol. **256**, 490 (2014).
8. M. Sheikholeslami, T. Hayat, A. Alsaedi, Int. J. Heat Mass Transf. **96**, 513 (2016).
9. M.M. Rahman, S. Mojumder, S. Saha, S. Mekhilef, R. Saidur, Int. Commun. Heat Mass Transf. **50**, 117 (2014).
10. H.A. Mohammed, K. Narrein, Int. Commun. Heat Mass Transf. **39**, 1375 (2012).
11. Mohsen Sheikholeslami, Kuppalapalle Vajravelu, Mohammad Mehdi Rashidi, Int. J. Heat Mass Transf. **92**, 339 (2016).
12. S. Masoud Hosseini, Leila Vafajoo, E. Ghasemi, B.H. Salman, Int. J. Heat Mass Transf. **93**, 228 (2016).
13. Mohammad Goharkhah, Mehdi Ashjaee, Mahmoud Shahabadi, Int. J. Thermal Sci. **99**, 113 (2016).
14. Noreen Sher Akbar, M. Raza, R. Ellahi, Eur. Phys. J. Plus **129**, 155 (2014).
15. M. Sheikholeslami, D.D. Ganji, J. Taiwan Inst. Chem. Eng. **65**, 43 (2016).
16. A. Zeeshan, R. Ellahi, M. Hassan, Eur. Phys. J. Plus **129**, 261 (2014).
17. M. Sheikholeslami, H.R. Ashorynejad, P. Rana, J. Mol. Liq. **214**, 86 (2016).
18. Mohsen Sheikholeslami, Davood Domiri Ganji, M. Younus Javed, R. Ellahi, J. Magn. & Magn. Mater. **374**, 36 (2015).
19. R. Ellahi, M. Hassan, A. Zeeshan, IEEE Trans. Nanotechnol. **14**, 726 (2015).
20. M. Sheikholeslami, D.D. Ganji, M.M. Rashidi, J. Magn. & Magn. Mater. **416**, 164 (2016).
21. Mohsen Sheikholeslami, Ali J. Chamkha, Numer. Heat Transf., Part A **69**, 1186 (2016).
22. M. Sheikholeslami, M.M. Rashidi, D.D. Ganji, J. Mol. Liq. **212**, 117 (2015).
23. M. Sheikholeslami, R. Ellahi, Int. J. Heat Mass Transf. **89**, 799 (2015).
24. Mohsen Sheikholeslami, Shirley Abelman, IEEE Trans. Nanotechnol. **14**, 561 (2015).
25. Mohsen Sheikholeslami Kandelousi, Eur. Phys. J. Plus **129**, 248 (2014).
26. Mohsen Sheikholeslami, Davood Domiri Ganji, Energy **75**, 400 (2014).
27. E.E. Tzirtzilakis, N.G. Kafoussias, J. Heat Transf. **132**, 011702 (2009).
28. H. Yamaguchi, *Engineering Fluid Mechanics* (Springer Science, Netherlands, 2008).

29. Ch. Kittel, *Introduction to Solid State Physics* (John Wiley & Sons, New York, 1967).
30. K.H.J. Buschow, *Handbook of Magnetic Materials* (Elsevier, 2003).
31. B.C. Pak, Y.I. Cho, Exp. Heat Transf. **11**, 151 (1998).
32. R.L. Hamilton, O.K. Crosser, Industr. Eng. Chem. Fund. **1**, 187 (1962).
33. M.B. Gerdroodbary, D.D. Ganji, Y. Amini, Acta Astron. **115**, 422 (2015).
34. M.B. Gerdroodbary, M. Imani, D.D. Ganji, Int. Commun. Heat Mass Transf. **64**, 42 (2015).
35. M.B. Gerdroodbary, M.R. Takami, H.R. Heidari, K. Fallah, D.D. Ganji, Acta Astron. **123**, 283 (2016).
36. M. Barzegar Gerdroodbary, Shock Waves **24**, 537 (2014).
37. D. Kim, Y. Kwon, Y. Cho, C. Li, S. Cheong, Y. Hwang, J. Lee, D. Hong, S. Moona, Curr. Appl. Phys. **9**, e119 (2009).
38. H. Aminfar, M. Mohammadpourfard, Y. Narmani Kahnamouei, J. Magn. & Magn. Mater. **323**, 1963 (2011).